Capillary Pressure and Wettability Behavior of CO_2 Sequestration in Coal at Elevated Pressures

Willem-Jan Plug, SPE, Horizon Energy Partners B.V.; **Saikat Mazumder,** SPE, Shell; and **Johannes Bruining,** SPE, Delft University of Technology

Summary

Enhanced coalbed-methane (ECBM) recovery combines recovery of methane (CH_4) from coal seams with storage of carbon dioxide (CO_2). The efficiency of ECBM recovery depends on the CO_2 transfer rate between the macrocleats, via the microcleats to the coal matrix. Diffusive transport of CO_2 in the small cleats is enhanced when the coal is CO_2-wet. Indeed, for water-wet conditions, the small fracture system is filled with water and the rate of CO_2 sorption and CH_4 desorption is affected by slow diffusion of CO_2. This work investigates the wetting behavior of coal using capillary pressures between CO_2 and water, measured continuously as a function of water saturation at in-situ conditions. To facilitate the interpretation of the coal measurements, we also obtain capillary pressure curves for unconsolidated-sand samples. For medium- and high-rank coal, the primary drainage capillary pressure curves show a water-wet behavior. Secondary forced-imbibition experiments show that the medium-rank coal becomes CO_2-wet as the CO_2 pressure increases. High-rank coal is CO_2-wet during primary imbibition. The imbibition behavior is in agreement with contact-angle measurements. Hence, we conclude that imbibition tests provide the practically relevant data to evaluate the wetting properties of coal.

Introduction

Geological sequestration (Orr 2004) of CO_2 is one of the viable methods to stabilize the concentration of greenhouse gases in the atmosphere and to satisfy the Kyoto protocol. The main storage options are depleted oil and gas reservoirs (Shtepani 2006; Pawar et al. 2004), deep (saline) aquifers (Kumar et al. 2005; Pruess et al. 2003; Pruess 2004), and unmineable coalbeds (Reeves 2001). Laboratory studies and recent pilot field tests (Mavor et al. 2004; Pagnier et al. 2005) demonstrate that CO_2 injection has the potential to enhance CH_4 production from coal seams. This technology can be used to sequester large volumes of CO_2, thereby reducing emissions of industrial CO_2 as a greenhouse gas (Plug 2007). The efficiency of CO_2 sequestration in coal seams strongly depends on the coal type, the pressure and temperature conditions of the reservoir (Siemons et al. 2006a, 2006b), and the interfacial interactions of the coal/gas/water system (Gutierrez-Rodriguez et al. 1984; Gutierrez-Rodriguez and Aplan 1984; Orumwense 2001; Keller 1987). It can be expected that in highly fractured coal systems the wetting behavior positively influences the efficiency of ECBM recovery. It is generally accepted that the coal structure consists of the macrocleat and fracture system (>50 nm) and the coal matrix (<50 nm). The macrofracture system is initially filled with water and provides the conduits where the mass flow is dominated by Darcy flow. The coal matrix can be subdivided in mesocleats (from 2 to 50 nm), microcleats (from 0.8 to 2 nm), and the micropores (<0.8 nm). The matrix system is relatively impermeable, and the mass transfer is dominated by diffusion. After a dewatering stage, CO_2 is injected and flows through the larger cleats of the coal. Subsequently, CO_2 is transported through the smaller cleats and is sorbed in the matrix blocks (Siemons et al. 2006a). Depending on the wettability of coal, we can distinguish the following gas exchange mechanisms:

- The coal is water-wet, and CO_2 and CH_4 diffuse in the water-filled cleats.
- The coal is CO_2-wet or gas-wet, and countercurrent capillary diffusion can take place.
- The coal is gas-wet, and binary diffusion of CO_2 and CH_4 occurs.

Capillary diffusion finds its origin in capillary pressure (P_c) effects, where P_c is defined as the pressure difference between the nonaqueous and aqueous phase. The storage rate for CO_2 is much smaller if the microcleat system is water-wet. This is because of the small CO_2 molecular-diffusion coefficient ($D_{CO_2} \approx 2\times10^{-9}$ m^2/s). For CO_2-wet conditions, a faster and more efficient sorption rate is expected and the molecular diffusion is much larger (i.e., $D_{CO_2} \approx 1.7\times10^{-7}$ m^2/s at 100 bar) (Bird et al. 1960). Therefore, we assert that the wettability of coal is important for ECBM recovery applications. For this reason, we have undertaken an experimental study to investigate the wetting properties of two different coal types under reservoir conditions, measuring the capillary pressure between CO_2 and water. The dissolution properties of CO_2 in water (Wiebe and Gaddy 1940), the interfacial tension between water and CO_2 (Chun and Wilkinson 1995), and the CO_2 sorption (Siemons et al. 2003) play important roles in the interpretation of capillary pressure experiments. The CO_2 will sorb on the coal and will cause a swelling-induced permeability decrease (Mazumder et al. 2006). The higher the pressure, the more CO_2 can be sorbed and the more the coal swells (Reucroft and Sethuraman 1987). The largest amount of sorption-induced swelling in intact coal is approximately 4%. It is found that the swelling for ground coal is much higher than intact coal and has been reported to be in the order of 15–20%. The swelling causes a porosity reduction, thus the water saturation decreases.

In the Background section, relevant literature about the wettability of coal and the capillary pressure is summarized. The Experimental Design section describes the experimental setup we have developed to measure the capillary pressure as a function of the CO_2 pressure. Furthermore, we describe the sample preparation and experimental procedure. In the Results and Discussion section, the experimental results are presented and discussed. We end with Conclusions.

Background

Wettability of Coal. Several methods exist to measure the wettability of rocks. We mention contact-angle measurements, imbibitions and forced displacement (Amott test), the US Bureau of Mines wettability method, and capillary pressure curves (Anderson 1986). Investigations of the wettability of coal reported in the literature are predominantly based on contact-angle measurements for coal/air/water systems at atmospheric pressures. In general, these measurements are performed by direct observations of drops attached to the solid viewed from one side (pendant-drop cell) (Siemons et al. 2006a).

Dry coal, like dry sand, is naturally hydrophobic, and its hydrophobicity varies from one sample to the other because of variations in coalification, genesis, and composition of coal (Gutierrez-Rodriguez et al. 1984). Previous studies (Gutierrez-Rodriguez et al. 1984; Gutierrez-Rodriguez and Aplan 1984; Orumwense 2001) were conducted to investigate the hydrophobicity of differ-

Original SPE manuscript received for review 1 November 2006. Revised manuscript received for review 6 December 2007. Paper (108161) peer approved 21 February 2008.

ent coal types. A comparative study of contact angles of air bubbles, oils, flocculants, and coagulant drops on flat, polished coal surfaces immersed in water was carried out by Orumwense (2001). From these experiments, a positive correlation between hydrophobicity and the coal rank of vitrinite-rich coals was found. It was also concluded that the hydrophobicity of coal decreased with decreasing fixed-carbon and total-carbon content. A series of experiments has been carried out by Gutierrez-Rodriguez et al. (1984) and Gutierrez-Rodriguez and Aplan (1984) with air and water for different coal types, varying from high to low rank. Qualitatively, the same results were reported as found by Orumwense (2001). Murata (1981) concluded that the contact angle depends on the hydrogen and oxygen content of the coal. Chi et al. (1988) observed an increasing contact angle between CO_2 and water on a coal surface with increasing pressures. Moreover, water-wet behavior was found when the ash content of the coal increased. Contact-angle measurements for the coal/CO_2/water system, using the pendant-drop cell, were carried out by Siemons et al. (2006a, 2006b). They concluded that wetting alteration from water-wet to CO_2-wet for high-rank coal already occurred at pressures above 2.7 bar. For medium-rank coal, the alteration was observed for pressures greater than 80 bar. The main reason for this wetting behavior was related to the difference in stability of the water film between the coal surface and the CO_2.

Capillary Pressure in Coal. The capillary pressure is defined as the pressure difference between the nonwetting phase and the wetting phase and is a function of the water saturation. In this study, we have measured the capillary pressure to investigate the wettability of the coal/CO_2/distilled water system at different CO_2 pressures in the range from 1 to 100 bar (Plug et al. 2006).

Conventional methodologies to determine capillary pressures are the porous-plate technique (Christoffersen and Whitson 1995), the micropore-membrane technique (Jennings et al. 1988; Longeron et al. 1995), mercury-drainage experiments (Anderson 1987), and the centrifuge method (Newsham et al. 2004). Conventional capillary pressure studies measure at static conditions (e.g., the multistep method) where an equilibrium water saturation (S_w) distribution is established (Hassanizadeh et al. 2002). Experimental data are also available in the literature for transient conditions, in which a continuous phase injection is applied (Kokkedee 1994; Wildenschild et al. 2001). Static P_c measurements are time-consuming; therefore, we choose the quasistatic approach. This method has the advantage that static P_c curves can be obtained for small flow rates [0.01 to 0.1 pore volumes (PV)/hour].

Capillary pressure measurements at reservoir conditions are reported mainly for the oil/water and the oil/gas system (Christoffersen and Whitson 1995), with the application to enhanced oil recovery. To our knowledge, capillary pressure between CO_2 and water in coal has not been investigated. Dabbous et al. (1976) measured the drainage capillary pressure between air and water of a Pocahontas and Pittsburgh coal at various pressure conditions. They found positive capillary pressure curves for both samples.

In this paper, we define drainage as injection of the nonaqueous phase to displace the water and define imbibition as the reverse process. These definitions are maintained regardless of the wetting conditions of the porous medium considered.

Experimental Design

Experimental Setup. The equipment is an optimized version of the setup presented in the work of Mazumder et al. (2003) and is based on the porous-plate technique combined with the micropore-membrane technique discussed extensively by Christoffersen and Whitson (1995); Jennings et al. (1988); Longeron et al. (1995); and Kokkedee (1994). A schematic of the setup is shown in **Fig. 1.** Two syringe pumps (Isco 260D) are connected to the inlet and outlet of the sample holder **(Fig. 2)** and can be set to a constant

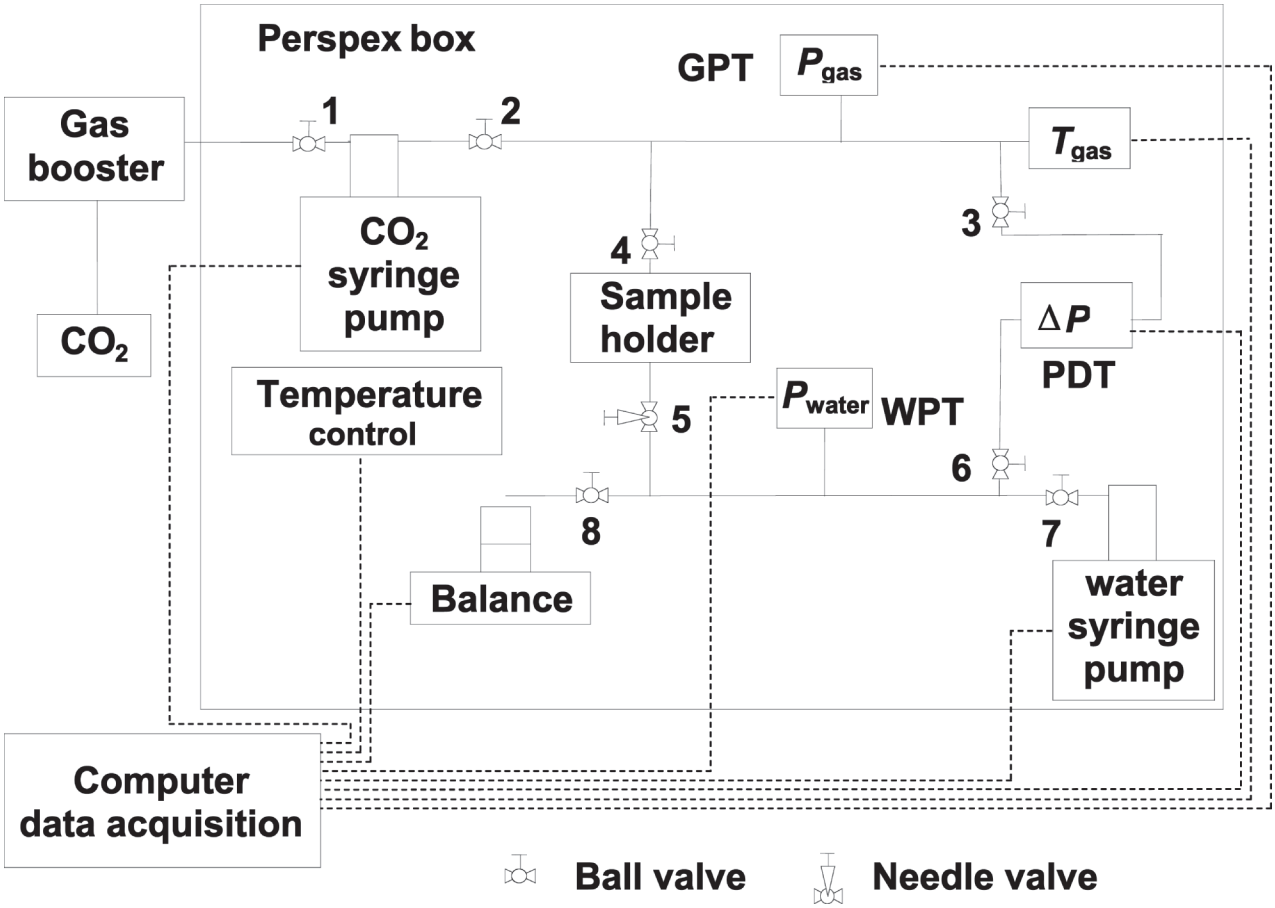

Fig. 1—Schematic layout of the setup.

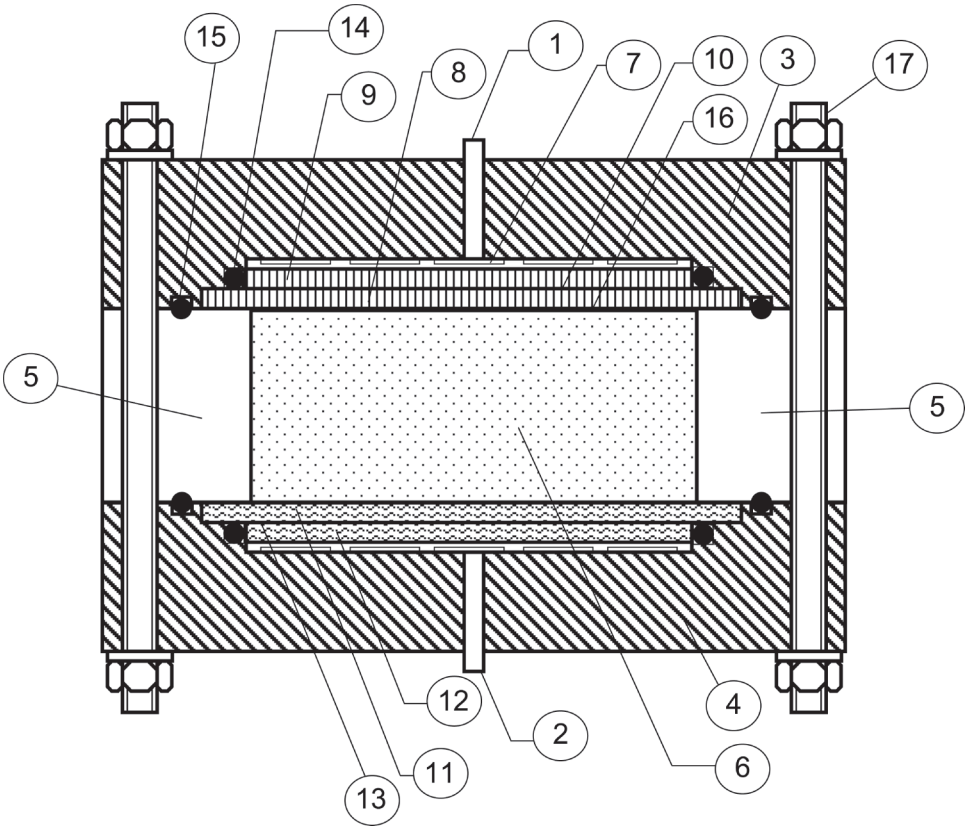

Fig. 2—Cross section of the sample holder: 1. gas-inlet; 2. water inlet; 3. stainless-steel endpiece 1; 4. stainless-steel endpiece 2; 5. stainless-steel ring (H=25 mm); 6. porous medium (D_{sample}=84 mm); 7. concentric grooves; 8. perforated plate ($D_{ss,1}$=90 mm); 9. perforated plate ($D_{ss,2}$=84 mm); 10. hydrophobic filter (D_g=90 mm , pore size=0.45 μm); 11. porous plate ($D_{s,1}$=90 mm); 12. porous plate ($D_{s,2}$=84 mm); 13. water-wet filter (D_w=90 mm, pore size=0.1μm); 14. O-rings (2.1 mm); 15. O-rings (4 mm); 16. nylon filter (pore size=210 μm); 17. stainless-steel bolts.

injection rate (±0.005 mL/h) or a constant pressure (±0.1 bar). The gas phase is injected or produced at the top of the sample holder, and the water is collected or injected at the bottom using the second syringe pump for pressures greater than 1 bar. For primary-drainage experiments at atmospheric conditions, Valve 7 is closed and Valve 8 is open and the water is produced in a beaker placed on a balance (±0.005 g). A layer of paraffin on top of the water prevents evaporation. The gas-pressure transducer (GPT) and the water-pressure transducer (WPT) record the single-phase pressures (0–100 bar, ±0.01 bar). The differential pressure between the gas and the water phase is measured by the pressure difference transducer (PDT), (0–500 mbar, ±0.1 mbar). This device is positioned at the same height as the middle of the sample such that no correction for gravity is required.

To maintain a constant temperature, we cover the entire setup with a Perspex box, sealed by polystyrene. Inside the box, two 60-W lightbulbs, which switch on and off, regulate the temperature from 25 to 40°C±0.5°C. We enable temperature equilibration for at least 2 days for gaseous and liquid CO_2/nitrogen (N_2) and at least 3 days when supercritical CO_2 is used.

The Sample Holder. The sample holder (Fig. 2) consists of a stainless-steel ring that contains the unconsolidated sample. The grains are kept in place using a combination of plates at the top and bottom of the sample. At the bottom, two porous plates with a permeability of 2×10^{-12} m^2 and a porosity of 0.32 support the sample and protect the hydrophilic membrane. Two stainless-steel plates, both with 32 perforations ($D_p = 5$ mm), are used at the top directly above the sample in combination with a nylon filter. Between the plates is the option to place a hydrophobic membrane for the primary-imbibition process, prohibiting water production (Fig. 2). To avoid leakage of gas or water over the hydrophobic or hydrophilic membranes, we seal the outer perimeter with an O-ring. Concentric flow grooves in the endpieces redistribute the injected and produced phase over the total sample area to avoid preferential flow and fast breakthrough of the injected phase.

Sample Description and Preparation. Four types of unconsolidated rock material are used—a fine-grained sand, a coarse-grained sand, a medium-rank coal, and a high-rank coal **(Table 1).** The first series of experiments is conducted on unconsolidated quartz sand using CO_2 and N_2 as the nonwetting phase. The fine-grained sand samples have an average grain size of $160<D_{50}<210$ μm. The capillary pressure curves are obtained to investigate the reproducibility and accuracy of the experimental technique. To facilitate the interpretation of the coal measurements, we obtain capillary pressure curves for unconsolidated coarse-sand samples with CO_2 and N_2 (Plug and Bruining 2007). These coarse samples ($360<D_{50}<410$ μm) have grain diameters comparable to the coal.

For the examination of the capillary pressure and wettability in coal, we have used the same two coal samples as described in the work of Siemons et al. (2006a, 2006b). The medium-rank Warndt-Luisenthal coal is high in volatile-matter content and low in fixed carbon content compared to the high-rank Selar-Cornish sample **(Table 2).** The coal samples are collected from a coal matrix, of which 2 kg of coal has been crushed in different grain-size fractions. For the coal experiments, we use grain-size fractions of $500<D_{50}<630$ μm. The moisture and ash content are determined according to the American Society for Testing and Materials 3173 and 3174 standard methods. Ground coal samples are used for the experiments to expose the relevant surface area to water and CO_2. Volumetric physisorption of CO_2 at 0°C was performed to determine the micropore area and micropore volume of the void space. These data are reported in Table 2 with the composition of the coal samples.

TABLE 1—CORRELATION BETWEEN THE EXPERIMENT NUMBERS AND THE EXPERIMENTAL PROPERTIES AND CONDITIONS

No.	Sample	Grain-Size (μm)	Gas	P (bar)	T (°C)	ϕ
1	Sand	$160 < D_{50} < 210$	CO_2	P_{atm}	23	0.36
2	Sand	$160 < D_{50} < 210$	CO_2	P_{atm}	21	0.34
3	Sand	$160 < D_{50} < 210$	CO_2	P_{atm}	22	0.35
4	Sand	$360 < D_{50} < 410$	CO_2	P_{atm}	23	0.36
4b	Sand	$360 < D_{50} < 410$	N_2	P_{atm}	24	0.37
5	Sand	$360 < D_{50} < 410$	CO_2	8	27	0.37
6	Sand	$360 < D_{50} < 410$	CO_2	85	27	0.37
7	Sand	$360 < D_{50} < 410$	CO_2	85	40	0.36
8	Sand	$360 < D_{50} < 410$	N_2	80	38	0.37
9	Warndt-Luisenthal	$500 < D_{50} < 630$	CO_2	87	27	0.43
10	Warndt-Luisenthal	$500 < D_{50} < 630$	CO_2	86	86	0.44
11	Warndt-Luisenthal	$500 < D_{50} < 630$	CO_2	86	86	0.43
12	Warndt-Luisenthal	$500 < D_{50} < 630$	CO_2	35	35	0.42
13	Selar-Cornish	$500 < D_{50} < 630$	CO_2	85	24	0.44
14	Selar-Cornish	$500 < D_{50} < 630$	CO_2	90	30	0.41
15	Selar-Cornish	$500 < D_{50} < 630$	CO_2	86	36	0.44
16	Selar-Cornish	$500 < D_{50} < 630$	CO_2	85	85	0.42
17	Selar-Cornish	$500 < D_{50} < 630$	CO_2	87	87	0.46
18	Selar-Cornish	$500 < D_{50} < 630$	CO_2	87	87	0.47
19	Selar-Cornish	$500 < D_{50} < 630$	CO_2	9	27	0.47

TABLE 2—COAL PROPERTIES OF THE MEDIUM- AND HIGH-RANK COAL

Sample	Warndt-Luisenthal	Selar-Cornish
Location	Saarbrücken, Germany	Selar, South Wales, UK
Stratigraphy	Westphalian C	Westphalian B
Proximate analysis		
Rank	hvBb*	Semianthracite
Moisture (%)	1.39	1.26
Volatile matter, w.f.** (%)	40.51	10.35
Ash, w.f. (%)	2.77	3.94
Fixed carbon, d.a.f.*** (%)	58.36	89.27
Ultimate analysis		
Carbon (C) (%)	81.3	85.68
Hydrogen (H) (%)	5.58	3.36
Nitrogen (%)	1.88	1.56
Sulfur (%)	0.69	0.68
Oxygen (O) (diff.) (%)	5.47	5.58
H/C	0.82	0.47
O/C	0.05	0.05
Coal petrology		
V_{max} (%)	0.71	2.41
Vitrinite	74.4	73.6
Liptinite	15.6	0
Inertinite	9	24.6
Minerals	1	1.8
Internal properties		
Specific surface (m^2/g)	104	208
Micropore volume (cm^3/g)	0.03545	0.071

* high volatile Bituminous b
** water-free
***dry, ash-free

Experimental Procedure. Before the start of each experiment, the setup is cleaned and the porous plates are dried. The assembling of the sample holder is from the bottom upward (Fig. 2). For each experiment, we use new hydrophilic filters and new O-rings. When Endpiece 2, including the porous plates and O-rings, and the stainless-steel ring are mounted together, we pour the unconsolidated sample into the sample holder. The sample is vibrated for 10 minutes to obtain a better packing. Finally, we put Endpiece 1, including the perforated plates, the hydrophobic filter, the nylon filter, and O-rings, on top of the stainless-steel ring. Now, the sample holder is placed in between Valves 4 and 5 (Fig. 1) and the entire system is evacuated for 1 hour. The porosity, ϕ, is determined with helium (Plug and Bruining 2007). For the sand and coal samples, we found a porosity of 0.34–0.37 and 0.42–0.47, respectively. Subsequently, the total system is again evacuated for 1 hour and filled with either water or gas.

When an experiment starts with the primary drainage process, the hydrophobic filter is left out. This makes it easier to pressurize the system. Through the high pressure, small air bubbles carried along with the distilled water are dissolved. In the same way, the hydrophilic filter is removed for primary imbibition tests. In this work, we consider three types of experiments:

Case 1—Primary Drainage at Atmospheric Pressure, $P=P_{atm}$. The total sample holder is initially filled with water from Valve 4 up to Valve 5 (Fig. 1). Subsequently, the water pump is used to apply a pressure of 10 bar to remove all possible air and to obtain 100% water saturation, and Valve 7 is closed. The gas tubing and pump are flushed and filled with either N_2 or CO_2. Finally, we set a constant temperature and let the system equilibrate. We open Valve 8, and the water pressure decreases toward atmospheric pressure. The primary drainage experiment starts when a constant gas-injection rate is applied and Valve 4 is opened. Because of operational restrictions of the syringe pumps for pressures less than 1 bar, no secondary imbibition tests are performed for atmospheric conditions.

Case 2—Primary Drainage and Secondary Imbibition at P>1 bar. For these experiments, the sample holder is filled initially with water and the water pump is set to the pressure we apply during the drainage experiment. Valve 4 is closed, and the gas tubing and pump are filled with either N_2 or CO_2. A gas booster, connected to Valve 1 (Fig. 1) is used to increase the gas pressure. We set a constant temperature and let the system equilibrate. Subsequently, when both the water and gas pressures are equal, a constant gas-injection rate is applied, the water pump is set to a constant pressure, and Valve 4 is opened. After the primary drainage process, the secondary imbibition process starts when the water pump is set to a constant injection rate and the gas pump is set to a constant production pressure. Since a constant water-injection rate is applied, the imbibition must be considered as a forced imbibition process.

Case 3—Primary Imbibition and Secondary Drainage at High Pressures, P>1 bar. The total sample holder is initially filled with gas from Valve 4 (open) up to Valve 5 (Fig. 1), and the water pump and tubing are filled and flushed with water. The absolute pressure is kept constant by the gas pump, and the water pressure in the tubing is increased using the water pump. We set a constant temperature and let the system equilibrate. The primary (forced) imbibition starts when a constant water-injection rate is applied, the gas pump is set to a constant pressure, and Valve 5 is opened. After the primary imbibition process, the secondary drainage process starts when the water pump is set to a constant production pressure and the gas pump is set to a constant injection rate.

Data Analysis. The capillary pressure used in this section is defined by the difference between the gas (CO_2/N_2) pressure and the water pressure and is measured directly by the PDT (Fig.1). In the analysis, no correction for the viscous pressure drop ($\Delta P_{visc} \approx \frac{\mu u \Delta z}{k_{eff}}$) has been made because ΔP_{visc} is negligible ($\approx 10^{-6}$ bar). Here, k_{eff} ($\approx 10^{-11}$ m^2) is derived from the harmonic average of the permeability of the (coal/sand) sample ($k_{sample} \approx 10^{-11}$ m^2), the porous plate, and the hydrophilic filter ($k_{filter} \approx 10^{-15}$ m^2). For the low capillary number ($Ca \approx 1 \times 10^{-10}$), the flow during the experiments is dominated by capillary forces.

The water saturation is obtained by the mass of water produced for the atmospheric conditions or by the change in volume of the water pump for high-pressure conditions (P>1 bar). Moreover, the integral mass balance is checked by weighing all the separate parts of the sample holder at the end of the experiment, from which an estimation of the final water saturation in the sample can be obtained.

For the high-pressure drainage experiments, the amount of water in the pump is measured to validate whether only negligible amounts of free gas are produced. For imbibition tests, we apply essentially the same procedure to validate that there is only negligible water production. It turns out that the gas volume in the water pump never exceeds 1% of the volume (Jennings et al. 1988). The capillary pressure curves are obtained on the basis of the following:

- The decrease (increase) in water saturation is derived from the mass/volume produced (injected).
- The initial water (gas) saturation for primary drainage (imbibition) is 1.
- The viscous pressure drop is neglected.
- For the drainage experiments, all the water from Endpiece 1 and the perforated plates is drained before the gas reaches the sample (Fig. 2).
- During the drainage process, all the water remains in pore space of the porous plates, in the hydrophilic filter, and in the void space of Endpiece 2 (Fig. 2).
- A sudden pressure drop marks the beginning of the primary imbibition process, independent of the water volume injected.
- Compressibility of water is neglected for all pressure conditions.
- The porosity and the permeability for all samples used are assumed constant during the drainage and imbibition processes.

Results and Discussion

We have tested the experimental method for both the fine- and coarse-grained unconsolidated-sand samples, applying different temperature and pressure conditions using either N_2 or CO_2. Moreover, a comprehensive analysis can be done by comparing the coal measurements with the results obtained for the coarse-sand sample. To clarify the correlation between the experiments and the numbering, an overview of the sample and system properties applied during the experiments is given in Table 1.

Capillary Pressure of the Unconsolidated-Sand/CO_2/Water System. Here, we describe the precision of the experimental method (Plug et al. 2007) and the influence of the applied flow rates on the P_c vs. S_w curves. The precision of the experimental procedure is estimated from the reproducibility of three experiments conducted on three different fine-sand samples at ambient conditions **(Fig. 3).** The highest precision (±1.5 mbar) is found for the intermediate water-saturation range ($0.4<S_w<0.8$). Near the endpoint saturations, the precision of the measurements is ±3 mbar.

In **Fig. 4,** Experiment 4 represents the capillary pressure curve between water and CO_2 at atmospheric conditions in coarse sand. During this experiment, the CO_2-injection rate is altered between 0 and 1 mL/h to investigate the influence of viscous forces and the possible dynamic behavior on P_c for the applied conditions. No significant effect in capillary pressure is observed for increasing or decreasing injection rates.

An additional atmospheric experiment, Experiment 4b, has been carried out for the N_2/water system in coarse sand (Fig. 4). The comparison between Experiments 4 and 4b is used to investigate the effect on the capillary pressure of CO_2 dissolution in water. This effect will be discussed further in the next section.

Primary Drainage and Secondary Imbibition in Coarse Sand. Drainage and imbibition curves have been measured for coarse-sand samples at elevated pressures and temperatures. A decrease in capillary pressure is measured for increasing CO_2 pressures (Fig. 4). This is a result of the pressure dependence of the interfacial

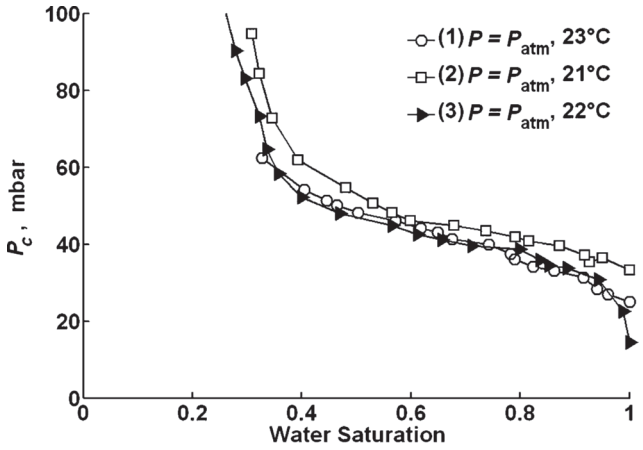

Fig. 3—Primary drainage capillary pressure curves for CO_2 injection in fine sand ($160<D_{50}<210$ μm) for atmospheric conditions. In each case, the CO_2-injection rate is 0.5 mL/h. The differences observed are an indication of the experimental precision.

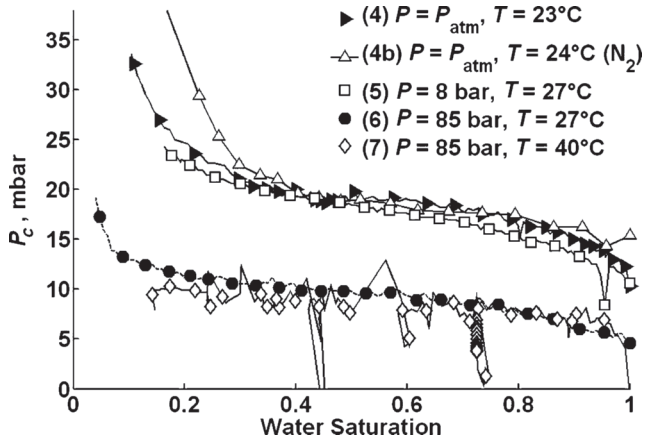

Fig. 4—Primary drainage capillary pressure curves for CO_2 and N_2 injection in coarse sand at various pressure and temperature conditions. The CO_2-injection rate is 0.5 mL/h for Experiments 5, 6, and 7. Varying CO_2- and N_2-injection rates are applied in Experiments 4 and 4b. The differences between the low- and high-pressure CO_2 experiments are ascribed to interfacial tension behavior.

tension (Chun and Wilkinson 1995). Hence, the capillary pressure curves can be scaled according to the interfacial tension (Plug and Bruining 2007). From Fig. 4, it can be seen that the capillary pressures for liquid CO_2 (Experiment 6) and supercritical CO_2 (Experiment 7) are of the same range.

The irregular behavior of the primary drainage curve obtained for Experiment 7 (Fig. 4) is ascribed to phase instabilities in the vicinity of the critical point. Small system perturbations, such as temperature variations and corresponding thermal-expansion effects, will cause occasional water imbibition during continuous CO_2 injection. Furthermore, for all cases, the capillary pressure is positive.

In **Fig. 5,** the secondary imbibition curves for Experiments 5 and 7 are presented. For supercritical conditions (Experiment 7), the imbibition process has stopped before the residual CO_2 saturation has been reached. A postmortem of Experiments 5 and 7 shows that no water is produced. A decrease in imbibition capillary pressure is observed for increasing CO_2 pressures. For $S_w>0.5$, the capillary pressure becomes negative for supercritical CO_2, indicating temporary CO_2-wet behavior. A tentative explanation for this behavior is that gas trapped in the crevices of the sand only slowly dissolves in the water. Therefore, the water will "see" a surface consisting of sand and gas patches (Plug and Bruining 2007). In contrast to the supercritical drainage curve, the corresponding secondary imbibition curve, shown in Fig. 5, is smooth. This implies that, for water-flow-controlled processes, the alternate drainage and imbibition effects do not occur.

The injection and production behavior for primary drainage with CO_2 under both atmospheric-pressure conditions and high-pressure conditions (85 bar) is presented in **Fig. 6.** Additionally, the cumulative injection and production volumes are shown for the atmospheric N_2 experiment (Experiment 4b). The difference between the injected and produced volumes for Experiment 4 (atmospheric pressure) is an indication for the dissolution effects of CO_2 in water. However, when liquid CO_2 is injected (Experiment 6), these effects are not observed and the cumulative gas volume injected is equal to the cumulative water volume produced (Plug and Bruining 2007).

The comparison between the atmospheric CO_2 and N_2 experiments (Experiments 4 and 4b) shows the large effect of the dissolution of CO_2 on the injection/production behavior. However, the capillary pressure is not influenced by dissolution effects, because the capillary pressure curves obtained for the CO_2/water and N_2/water systems (Fig.4) are of the same range (Plug and Bruining 2007).

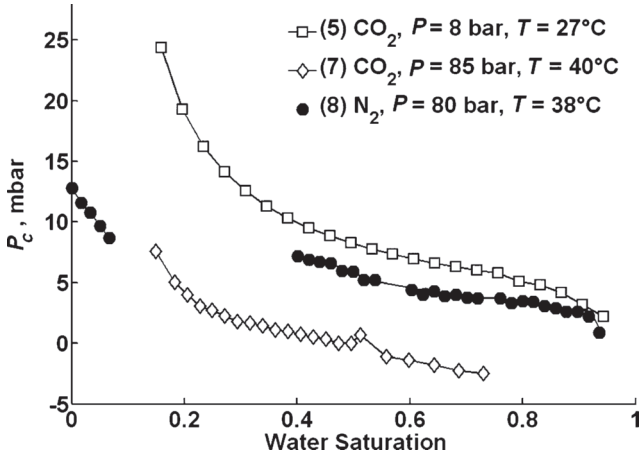

Fig. 5—Secondary imbibition capillary pressure curves in coarse sand for the sand/CO_2/water system (Experiments 5 and 7) and the primary imbibition curve for the sand/N_2/water system (Experiment 8) at various pressure and temperature conditions. In each case, the water-injection rate is 0.5 mL/h. Note that, for Experiment 7, the capillary pressure becomes negative for $S_w>0.5$.

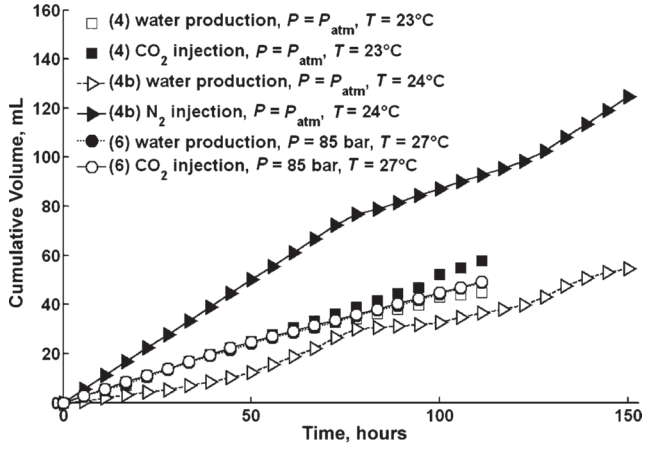

Fig. 6—Cumulative water production and gas injection for drainage experiments in coarse sand with gaseous CO_2 (Experiment 4, varying CO_2-injection rates), gaseous N_2 (Experiment 4b), and liquid CO_2 (Experiment 6, CO_2-injection rate of 0.5 mL/h). Note that the water-production and CO_2-injection curves for 85 bar coincide.

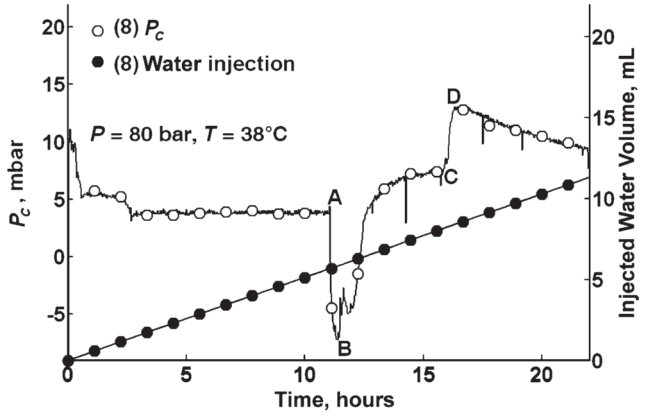

Fig. 7—Evolution of the capillary pressure and the cumulative water injection for the primary imbibition process with N_2 (Experiment 8, water-injection rate is 0.5 mL/h). This plot shows the typical behavior for a primary imbibition experiment.

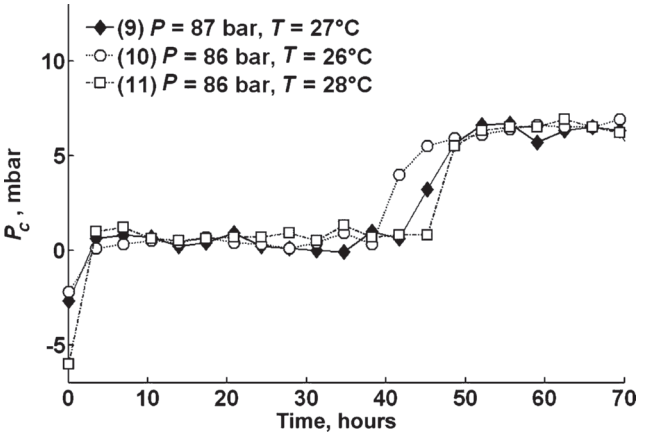

Fig. 8—History of the capillary pressure for primary drainage in medium-rank coal. In all cases, the liquid-CO_2-injection rate is 0.5 mL/h. These experiments show the reproducibility at high CO_2 pressures in coal. The sudden increase in P_c indicates the start of the primary drainage.

Primary Imbibition in Coarse Sand. We have investigated the properties of the setup during primary imbibition processes. Therefore, an imbibition experiment is conducted for the coarse-sand/N_2/water system (Fig. 5, Experiment 8). **Fig. 7** plots the capillary pressure and the cumulative water injection vs. time for the period before the imbibition process. Distinct events can be observed: The capillary pressure drops rapidly when the water reaches the porous plates (A) and subsequently rises toward a stable situation (B), where water is imbibing in the porous plates until (C). The pressure difference increases rapidly when the water starts to imbibe in the sample (D). From the water-balance computation, we determine that only 15% of the pore space of the porous plates is saturated. We obtain the water saturation after (D), assuming that the total volume of water injected from this moment is present as pore water in the sample. The corresponding primary imbibition curve of Experiment 8 is presented in Fig. 5. The imbibition capillary pressure curve is positive, and the residual N_2 saturation is 0.16. Because the hydrophobic filter is used, no water can be produced in the gas pump. For the water saturation range of $0.1<S_w<0.4$, the data acquisition system has failed.

Capillary Pressure and Wettability for the Coal/CO_2/Water System. ***Medium-Rank Coal.*** **Fig. 8** shows the reproducibility for drainage experiments for the Warndt-Luisenthal coal (medium rank) for liquid CO_2 (Experiments 9, 10, and 11). The moment the CO_2 has entered the sample and the capillary entry pressure has been reached is comparable for all three cases. As a result of the water production at the beginning of the experiments, small differences in starting times occur. The difference in initial water production is caused by the initial pressure difference between the water and CO_2 pump. However, as can be seen in **Fig. 9,** the influence on the capillary pressure saturation behavior of the water-production evolution before the drainage process is hardly visible. For both liquid CO_2 and gaseous CO_2 (Experiment 12), positive drainage capillary pressures are measured. The positive sign means that the medium-rank coal is water-wet during the drainage process because a water film exists between the coal surface and the advancing CO_2. This film prevents the exposure of the coal surface to CO_2. Similar to the sand experiments (Fig. 4), the differences in drainage capillary pressure are directly related to the interfacial tension, as reported by Chun and Wilkinson (1995). More information is obtained when the CO_2 injection rate is set to zero (Experiment 11, A and B in Fig. 9). During these equilibration steps at $S_w = 0.81$ and $S_w = 0.38$, respectively, the capillary pressure decreases toward zero **(Fig. 10).** Because no dynamic or viscous behavior is observed for the capillary pressure during continuous CO_2 injection, the decrease in P_c must be ascribed to another process. A plausible explanation for this behavior is that the surface-wetting film is ruptured by the presence of the high-pressure CO_2 (Hirasaki 1991). Because the rupture of wetting films can be a slow process, this CO_2-wet behavior will not necessarily

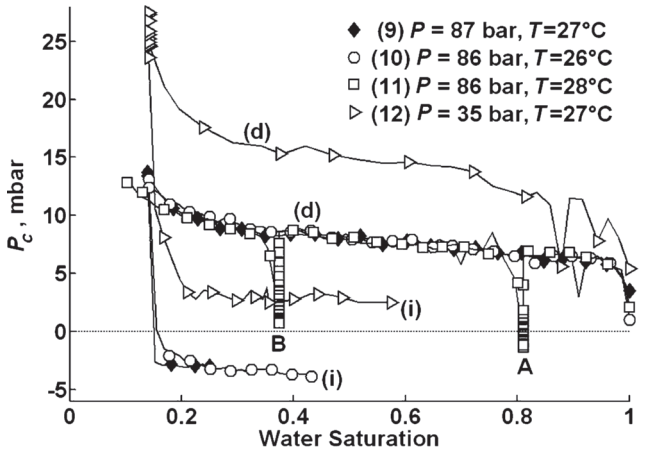

Fig. 9—Primary drainage (d) and secondary imbibition curves (i) obtained for the medium-rank coal. The CO_2-injection rate for Experiments 9, 10, and 11 is 0.5 mL/h and it is 1 mL/h for Experiment 12. The water-injection rate during secondary imbibition is 0.5 mL/h in all cases. These results suggest that imbibition experiments are a good indication of wettability effects.

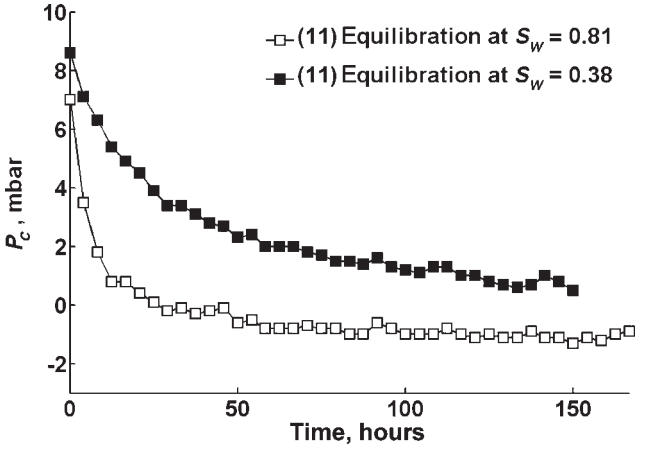

Fig. 10—Equilibration of P_c during a primary drainage experiment with liquid CO_2 in Warndt- Luisenthal coal (Experiment 11) at two different water saturations.

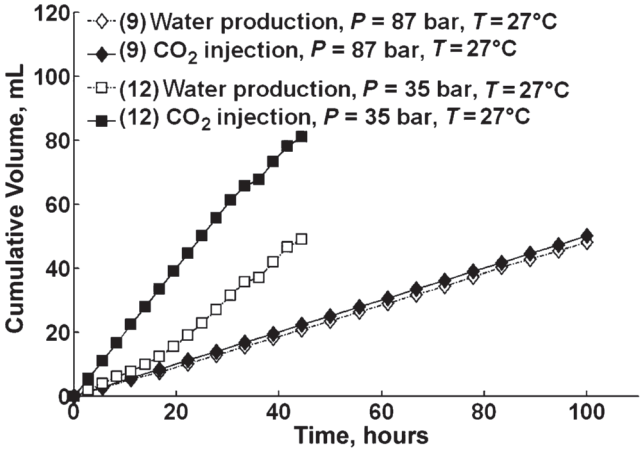

Fig. 11—Cumulative water production and CO_2 injection for primary drainage experiments with liquid CO_2 in medium-rank coal (Experiment 9, CO_2-injection rate is 0.5 mL/h) and gaseous CO_2 in medium-rank coal (Experiment 12, CO_2-injection rate is 1 mL/h). Significant discrepancy between the water production and CO_2 injection is observed only for gaseous-CO_2 conditions.

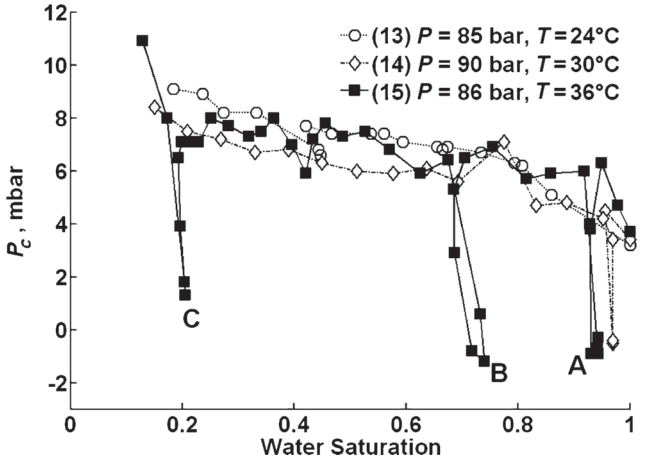

Fig. 12—Primary drainage capillary pressure curves for CO_2 injection in high-rank Selar-Cornish coal. The CO_2 injection rate is 0.5 ml/h in each case. Sudden imbibition events during CO_2 injection are indicated by A, B and C.

be observed in the time frame of our experiments or even in field applications.

The results for the secondary imbibition process for the medium-rank coal are shown in Fig. 9. A decrease of the secondary imbibition capillary pressure from positive to negative is observed for increasing CO_2 pressures. Because negative interfacial tensions are excluded (Chun and Wilkinson 1995), this change in sign is ascribed to the wettability alteration from water-wet (P_c>0) to CO_2-wet (P_c<0). The reproducibility of the capillary behavior in the medium-rank coal can be estimated from Experiments 9, 10, and 11 (Fig. 9) and is also applicable for the 35-bar drainage experiment (Fig. 9, Experiment 12).

The results are in agreement with the pressure-dependent wettability of the medium-rank coal discussed by Siemons et al. (2006b). They measured increasing contact angles (θ) for increasing CO_2 pressures for the medium-rank-coal/CO_2/water system where the crossover from water-wet (θ<90°) to CO_2-wet (θ>90°) behavior occurs in the range of 80 to 85 bar.

Comparison of the secondary imbibition curves measured for the medium-rank coal and for coarse sand (Experiment 7, Fig. 5) shows that the capillary pressure in coal immediately drops to a negative value, indicating that no spontaneous imbibition takes place. This behavior is not observed for the water-wet sand (Experiment 7), which shows a gradual decrease of the secondary imbibition capillary pressure.

The wetting alteration of the medium-rank coal is also emphasized by the water-production behavior. Early water breakthrough is observed for pressures greater than 85 bar (Experiments 9 and 10). No water was produced for the gaseous CO_2 experiment (Experiment 12). At the end of this experiment, we have aborted the imbibition process before the residual-gas saturation has been reached. As opposed to the corresponding experiments in coal (Experiments 9 and 10), no water breakthrough is observed during the secondary imbibition experiment in the coarse sand (Experiment 7, Fig. 5).

The production and injection curves for the primary drainage in medium-rank coal at 35 and 87 bar (Experiments 12 and 9, respectively) are presented in **Fig. 11.** The same conditions as those in Experiment 9 are applied for Experiment 6 (primary drainage in coarse sand, Fig. 6). Comparison of the water production vs. gas injection for Experiments 6 and 9 shows that the effect of CO_2 sorption in coal on the production behavior is negligible. Similar to the drainage experiment in coarse sand, the cumulative-production and -injection curves for coal are parallel. The deviation in cumulative volumes at the end of the drainage process is $\Delta V = 0.36$ mL and $\Delta V = 1.45$ mL for the sand and the medium-rank coal, respectively. We also mention that the amount of sorbed CO_2 on the coal is difficult to determine because of the sorption of CO_2 in the O-rings.

High-Rank Coal. Primary drainage curves for the high-rank Selar-Cornish coal at pressures between 85 and 90 bar and temperatures varying from 24 to 36°C are shown in **Fig. 12.** In all drainage cases, the high-rank coal shows water-wet behavior because the P_c vs. S_w curves are positive. In contrast to the high-pressure drainage experiments conducted on the medium-rank coal (Fig. 9), the P_c vs. S_w curves are irregular, especially when the temperature approaches or becomes higher than the critical temperature of CO_2. The imbibition events (denoted by A, B, and C in Fig. 12) occurring in Experiment 15 are also observed during the primary drainage with supercritical CO_2 in sand (Experiment 7, Fig. 4).

We also have conducted a series of primary imbibition experiments on the high-rank coal, and the results are presented in **Fig. 13.** Here, the primary imbibition measurement conducted for the sand/N_2/water system (Experiment 8, Fig. 5) is used as a reference to indicate the time when the imbibition process starts. Fig. 13 plots the primary imbibition curves for the high-rank coal. Negative capillary pressures are measured for both gaseous CO_2 (9 bar and 27°C) and supercritical CO_2 (from 85 to 87 bar, 40°C). It is clear from Fig. 13 that the capillary pressure behavior for supercritical CO_2 is also irregular under imbibition conditions,

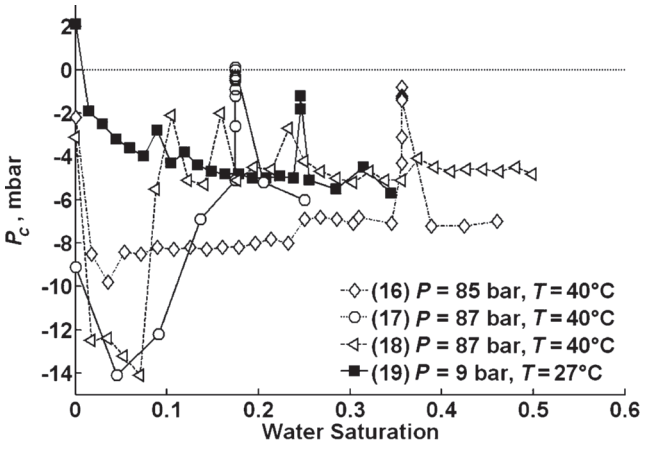

Fig. 13—Primary imbibition capillary pressure curves in high-rank Selar-Cornish coal for supercritical CO_2 (Experiments 16, 17, and 18) and gaseous CO_2 (Experiment 19). The water-injection rate is 0.5 mL/h in each case. The reason for the capillary pressure behavior for S_w<0.1 is not yet clear.

which are caused by sudden drainage events. The average magnitude of the imbibition P_c is approximately –8 mbar for Experiment 16 and approximately –5 mbar for Experiments 17, 18, and 19. The capillary pressure in the water saturation range of $0<S_w<0.1$ shows a distinct character for Experiments 17 and 18. The reasons for this are not yet clear.

For all pressure conditions, the high-rank coal shows CO_2-wet behavior during imbibition, which again is emphasized by the fast water breakthrough occurring at $S_w<0.5$.

From the imbibition results of Experiment 12 (Fig. 9) and Experiment 19 (Fig. 13), it is clear that the high-rank coal compared to the medium-rank coal is CO_2-wet for much lower CO_2 pressures. Our results are in agreement with the findings described by Siemons et al. (2006a). For the high-rank coal, they found a wetting alteration for system pressures higher than 2.6 bar.

Although we have not measured secondary imbibition curves for the high-rank coal, it can be expected that CO_2-wet behavior will also be observed. In general, the wetting behavior, with respect to the carbon content and the rank of the coal (Table 2), corresponds to the results obtained by Gutierrez-Rodriguez et al. (1984), Gutierrez-Rodriguez and Aplan (1984), and Orumwense (2001). It appears that imbibition experiments provide good qualitative information regarding the wettability of coal. This implies that the water-saturation history plays an important role for the wetting characteristics of coal (Private communication with M. Blunt, 16th International Conference on Computational Methods in Water Resources, 18–22 June 2006, Copenhagen).

Conclusions

- A capillary pressure setup has been developed and validated that can be used to determine the wettability of the coal/CO_2/water system as a function of the system pressure.
- The interpretation of the complex coal experiments can be facilitated by comparison of the sand/CO_2/water and coal/CO_2/water experiments at a range of pressure and temperature conditions. The reproducibility of the experiments is considered good.
- Increasing CO_2 pressures result in decreasing primary drainage capillary pressures for all samples used. This can be explained by the decrease in interfacial tension (Chun and Wilkinson 1995).
- Both the medium- and high-rank coal are water-wet during the primary drainage process.
- With increasing system pressures, the wettability of the medium-rank coal changes from water-wet to CO_2-wet. High-rank coal is CO_2-wet during primary imbibition experiments in the entire pressure range. The behavior during imbibition corresponds to contact-angle data (Siemons et al. 2006a).
- Fast water breakthrough during the imbibition process indicates CO_2-wet behavior.
- Imbibition tests provide relevant data to evaluate the wetting properties of coal.
- The difference between imbibition and drainage experiments can be explained by the stability of a water layer on the coal. Such a film must be ruptured (Hirasaki 1991) before the coal becomes CO_2-wet.
- This film rupture may imply that the time scale in laboratory experiments is not representative of field-scale behavior.

Nomenclature

D_{CO_2} = molecular-diffusion coefficient of CO_2, m^2/s
D_{sample} = sample diameter, mm
D_g = diameter of hydrophobic filter, mm
D_p = diameter of perforations, mm
D_s = diameter of porous plate, mm
D_{ss} = diameter of perforated plate, mm
D_w = diameter of hydrophilic filter, mm
D_{50} = average particle size, μm
H = sample height, mm
P = pressure, bar
P_{atm} = atmospheric pressure, bar
P_c = capillary pressure, mbar
S_w = water saturation
t = time, s
T = temperature, °C
θ = contact angle, degrees
ϕ = porosity

Acknowledgments

The research presented in this work was carried out as part of the CO_2 Capture, Transport, and Storage (CATO) program in the Netherlands (http://www.co2-cato.nl). The financial support is gratefully acknowledged. We thank A. Hoving, L. Vogt, P.S.A. de Vreede, and H.G van Asten for their technical support. We thank Dr. K.H.A.A. Wolf for insightful discussions on coal behavior.

References

Anderson, W.G. 1986. Wettability Literature Survey—Part 2: Wettability Measurement. *JPT* **38** (11): 1246–1262. SPE-13933-PA. DOI: 10.2118/13933-PA.

Anderson, W.G. 1987. Wettability Literature Survey—Part 4: Effects of Wettability on Capillary Pressure. *JPT* **39** (10): 1283–1300. SPE-15271-PA. DOI: 10.2118/15271-PA.

Bird, R.B., Steward, W.E., and Lightfoot, E.N. 1960. *Transport Phenomena*. New York City: John Wiley and Sons.

Chi, S.M., Morsi, B.I., Klinzing, G.E., and Chiang, S.H. 1988. Study of interfacial properties in the liquid CO_2-water-coal system. *Energy Fuels* **2** (2): 141–145. DOI:10.1021/ef00008a007.

Christoffersen, K.R. and Whitson, C.H. 1995. Gas/Oil Capillary Pressure of Chalk at Elevated Pressures. *SPEFE* **10** (3): 153–159. SPE-26673-PA. DOI: 10.2118/26673-PA.

Chun, B.-S. and Wilkinson, G.T. 1995. Interfacial tension in high-pressure carbon dioxide mixtures. *Ind. Eng. Chem. Res.* **34** (12): 4371–4377. DOI:10.1021/ie00039a029.

Dabbous, M.K., Reznik, A.A., Mody, B.G., Fulton, P.F., and Taber, J.J. 1976. Gas-Water Capillary Pressure in Coal at Various Overburden Pressures. *SPEJ* **16** (5): 261–268; *Trans.,* AIME, **261.** DOI: 10.2118/5348-PA.

Gutierrez-Rodriguez, J.A. and Aplan, F.F. 1984. The effect of oxygen on the hydrophobicity and floatability of coal. *Colloids and Surfaces* **12:** 27–51. DOI:10.1016/0166-6622(84)80087-6.

Gutierrez-Rodriguez, J.A., Purcell, R.J. Jr., and Aplan, F.F. 1984. Estimating the hydrophobicity of coal. *Colloids and Surfaces* **12:** 1. DOI:10.1016/0166-6622(84)80086-4.

Hassanizadeh, S.M., Celia, M.A., and Dahle, H.K. 2002. Dynamic effect in the capillary pressure-saturation relationship and its impacts on unsaturated flow. *Vadose Zone J.* **1** (1): 38–57.

Hirasaki, G.J. 1991. Wettability: Fundamentals and Surface Forces. *SPEFE* **6** (2): 217–226; *Trans.,* AIME, **291.** SPE-17367-PA. DOI: 10.2118/17367-PA.

Jennings, J.R. Jr., McGregor, D.S, and Morse, R.A. 1988. Simultaneous Determination of Capillary Pressure and Relative Permeability by Automatic History Matching. *SPEFE* **3** (2): 322–328. SPE-14418-PA. DOI: 10.2118/14418-PA.

Keller, D.V. Jr. 1987. The contact angle of water on coal. *Colloids and Surfaces* **22** (1): 21–35. DOI:10.1016/0166-6622(87)80003-3.

Kokkedee, J.A. 1994. Simultaneous Determination of Capillary Pressure and Relative Permeability of a Displaced Phase. Paper SPE 28827 presented at the European Petroleum Conference, London, 25–27 October. DOI: 10.2118/28827-MS.

Kumar, A., Ozah, R., Noh, M.K., Pope, G.A., Bryant, S., Sepehrnoori, K., and Lake, L.W. 2005. Reservoir Simulation of CO_2 Storage in Deep Saline Aquifers. *SPEJ* **10** (3): 336–348. SPE-89343-PA. DOI: 10.2118/89343-PA.

Longeron, D., Hammervold, W.L., and Skjaeveland, S.M. 1995. Water-Oil Capillary Pressure and Wettability Measurements Using Micropore Membrane Technique. Paper SPE 30006 presented at the International Meeting on Petroleum Engineering, Beijing, 14–17 November. DOI: 10.2118/30006-MS.

Mavor, M.J., Gunter, W.D., and Robinson, J.R. 2004. Alberta Multiwell Micro-Pilot Testing for CBM Properties, Enhanced Methane Recovery and CO_2 Storage Potential. Paper SPE 90256 presented at the SPE

Annual Technical Conference and Exhibition, Houston, 26–29 September. DOI: 10.2118/90256-MS.

Mazumder, S., Karnik, A., and Wolf, K.H. 2006. Swelling of Coal in Response to CO_2 Sequestration for ECBM and its Effect on Fracture Permeability. *SPEJ* **11** (3): 390–398. SPE-97754-PA. DOI: 10.2118/97754-PA.

Mazumder, S., Plug, W.-J., and Bruining, J. 2003. Capillary Pressure and Wettability Behavior of Coal-Water-Carbon Dioxide System. Paper SPE 84339 presented at the SPE Annual Technical Conference and Exhibition, Denver, 5–8 October. DOI: 10.2118/84339-MS.

Murata, T. 1981. Wettability of coal estimated from the contact angle. *Fuel* **60** (8): 744–746. DOI:10.1016/0016-2361(81)90230-1.

Newsham, K.E., Rushing, J.A., Lasswell, P.M., Cox, J.C., and Blasingame, T.A. 2004. Comparative Study of Laboratory Techniques for Measuring Capillary Pressures in Tight Gas Sands. Paper SPE 89866 presented at the SPE Annual Technical Conference and Exhibition, Houston, 26–29 September. DOI: 10.2118/89866-MS.

Orr, F.M. Jr. 2004. Storage of Carbon Dioxide in Geologic Formations. *JPT* **56** (9): 90–97. SPE-88842-PA. DOI: 10.2118/88842-PA.

Orumwense, F.F.O. 2001. Wettability of coal—A comparative study. *Scandinavian J. of Metallurgy* **30** (4)**:** 204–211. DOI:10.1034/j.1600-0692.2001.300402.x.

Pagnier, H.J.M., van Bergen, F., Kreft, E., van der Meer, L.G.H., and Simmelink, H.J. 2005. Field Experiment of ECBM-CO_2 in the Upper Silesian Basin of Poland (RECOPOL). Paper SPE 94079 presented at the SPE Europec/EAGE Annual Conference, Madrid, Spain, 13–16 June. DOI: 10.2118/94079-MS.

Pawar, R.J., Warpinski, N.R., Benson, R.D., Grigg, R.B., Krumhansl, J.L., and Stubbs, B.A. 2004. Geologic Sequestration of CO_2 in a Depleted Oil Reservoir: An Overview of a Field Demonstration Project. Paper SPE 90936 presented at the SPE Annual Technical Conference and Exhibition, Houston, 26–29 September. DOI: 10.2118/90936-MS.

Plug W.-J. 2007. Measurements of capillary pressure and electric permittivity of gas-water systems in porous media at elevated pressures; Application to geological storage of CO_2 in aquifers and wetting behavior in coal. PhD thesis, Delft University of Technology, Delft, The Netherlands.

Plug, W.-J. and Bruining, J. 2007. Capillary pressure for the sand–CO_2–water system under various pressure conditions. Application to CO_2 sequestration. *Advances in Water Resources* **30** (11): 2339–2353. DOI:10.1016/j.advwatres.2007.05.010.

Plug, W.-J., Mazumder, S., Bruining, J., Siemons, N., and Wolf, K.H. 2006. Capillary pressure and wettability behavior of the coal-water-carbon dioxide system at high pressures. Paper 606 presented at the International CBM Symposium, Tuscaloosa, Alabama, USA, 22–26 May.

Plug, W.-J., Slob, E., Bruining, J., and Tirado, L.M.M. 2007. Simultaneous measurement of hysteresis in capillary pressure and electric permittivity for multiphase flow through porous media. *Geophysics* **72** (3): A41. DOI:10.1190/1.2714684.

Pruess, K. 2004. Numerical Simulation of CO_2 Leakage From a Geologic Disposal Reservoir, Including Transitions From Super- to Subcritical Conditions, and Boiling of Liquid CO_2. *SPEJ* **9** (2): 237–248. SPE-86098-PA. DOI: 10.2118/86098-PA.

Pruess, K., Xu, T., Apps, J., and Garcia, J. 2003. Numerical Modeling of Aquifer Disposal of CO_2. *SPEJ* **8** (1): 49–60. SPE-83695-PA. DOI: 10.2118/83695-PA.

Reeves, S.R. 2001. Geological Sequestration of CO_2 in Deep, Unmineable Coalbeds: An Integrated Research and Commerical-Scale Field Demonstration Project. Paper SPE 71749 presented at the SPE Annual Technical Conference and Exhibition, New Orleans, 30 September–3 October. DOI: 10.2118/71749-MS.

Reucroft, P.J. and Sethuraman, A.R. 1987. Effect of pressure on carbon dioxide induced coal swelling. *Energy Fuels* **1** (1): 72–75. DOI:10.1021/ef00001a013.

Shtepani, E. 2006. CO_2 Sequestration in Depleted Gas/Condensate Reservoirs. Paper SPE 102284 presented at the SPE Annual Technical Conference and Exhibition, San Antonio, Texas, USA, 24–27 September. DOI: 10.2118/102284-MS.

Siemons N., Busch, A., Bruining, H., Krooss, B., and Gensterblum, Y. 2003. Assessing the Kinetics and Capacity of Gas Adsorption in Coals by a Combined Adsorption/Diffusion Method. Paper SPE 84340 presented at the SPE Annual Technical Conference and Exhibition, Denver, 5–8 October. DOI: 10.2118/84340-MS.

Siemons N., Bruining, H., Wolf, K.-H., and Plug, W.-J. 2006a. Pressure Dependence of the CO_2 Contact Angle on Bituminous Coal and Semi-Anthracite in Water. Paper 0605 presented at the International CBM Symposium, Tuscaloosa, Alabama, USA, 22–26 May.

Siemons N. et al. 2006b. Pressure dependence of the contact angle in a CO_2-H_2O-coal system. *J. Coll. Int. Sci.* **297** (2)**:** 755–761. DOI:10.1016/j.jcis.2005.11.047.

Wiebe, R. and Gaddy, V.L. 1940. The solubility of carbon dioxide in water at various temperatures from 12 to 40°C and at pressures to 500 atmospheres. Critical phenomena. *J. Am. Chem. Soc.* **62** (4): 815–817. DOI:10.1021/ja01861a033.

Wildenschild, D., Hopmans, J., and Simunek, J. 2001. Flow rate dependence of soil hydraulic characteristics. *Soil Sci. Soc. Am. J.* **65** (1): 35–48.

SI Metric Conversion Factors

cp × 1.000	E–03* = Pa·s
ft × 3.048	E–01* = m
md × 9.869 233	E–04 = μm^2
psi × 6.8948	E–03* = MPa

*Conversion factor is exact.

Willem-Jan Plug has worked since 2006 as a reservoir engineer for Horizon Energy Partners B.V., an oil and gas consultancy company in The Hague. He holds an MS degree in civil engineering and a PhD degree in petroleum engineering from Delft University of Technology. His special interests are geological sequestration of CO_2, theoretical and experimental aspects of (multiphase) flow in porous media and near-surface geophysics. **Saikat Mazumder** has worked with Oil and Natural Gas Corporation Ltd. (ONGC), India, as a production geologist in drilling and production testing of primary coalbed methane wells. He holds an MS degree in applied geology from Indian School of Mines, specializing in coal cleat characterization and its effect on CBM production. He is pursuing a PhD degree at Delft University of Technology on the dynamics of CO_2 in coal. He worked on reservoir engineering aspects of ECBM and high-pressure flow experiments, coal swelling and modeling anomalous diffusion. Since 2006, Mazumder has been working as a technical specialist for global CBM and ECBM aspirations of Shell. His present area of focus is Indonesia, Australia, China, Botswana, and India. **Hans Bruining** is professor of geoenvironmental engineering at the Technical University of Delft. He holds a PhD degree from the University of Amsterdam. He is one of the founders of the Dietz-De Josselin de Jong laboratory. His special interests are the environmental aspects of fossil fuel recovery, enhanced oil recovery, and the theory and experiments of complex flow processes in porous media. He is review chairman of SPEJ.